Contrasting lithospheric signatures across the western United States revealed by Sp receiver functions

Vedran Lekić [a,*], Karen M. Fischer [b]

[a] Department of Geology, University of Maryland, College Park, MD 20742, USA
[b] Department of Geological Sciences, Brown University, Providence, RI 02912, USA

A B S T R A C T

To explore how lithospheric structure varies between tectonic and magmatic terranes of the western United States, we use observations of shear-to-compressional wave conversions across lithospheric velocity interfaces. With a newly developed automatic method designed to take advantage of the EarthScope Transportable Array and other broadband seismic arrays deployed across the region, and an optimized deconvolution technique based on the extended-time multi-taper method, we map variations in the depth to the seismic Moho, lithosphere–asthenosphere boundary (LAB) and mid-lithospheric discontinuities (MLDs). Beneath areas that have undergone substantial extension in the Neogene—including the eastern Great Basin, the southern Basin and Range, and the southern Rio Grande Rift—we detect strong Sp conversions across a relatively shallow (60–80 km) seismically-defined LAB. We detect Sp conversions across an 80–90 km depth discontinuity beneath the High Rockies, which we interpret as the seismically-defined LAB. Beneath areas that have remained relatively undeformed—including the Wyoming craton and the Great Plains craton—we detect Sp conversions in the 90–140 km depth range that are substantially weaker and more distributed in depth than those beneath less stable regions. Beneath the Colorado Plateau, Sp CCP stacks show that lithospheric thinning has accompanied magmatic encroachment and the LAB beneath the margins of the Plateau is indistinguishable from the LAB of the surrounding extensional provinces. In contrast, beneath central and northern Colorado Plateau, weaker Sp conversions are observed in the 90–140 km depth range. The observed variations in lithospheric structure across structural blocks with different magmatic and deformational histories imply that: (1) both mechanical thinning and magmatic and thermal erosion have likely contributed to the thin lithosphere observed in the Basin and Range and southern Rio Grande Rift; (2) at the margins of the Colorado Plateau and beneath the High Rockies, where extension has been relatively minor, strong and shallow seismic LABs indicate magmatic alteration of the lithosphere; (3) MLDs seen in comparatively thick, stable lithosphere produce weaker Sp conversions and are often more distributed in depth than seismically-observed LABs in regions of thin lithosphere; (4) MLDs and weak, deep phases consistent with a seismic LAB are sometimes observed together.

© 2013 Elsevier B.V. All rights reserved.

1. Introduction

Variations in thickness of the continental lithosphere are genetically related to deformation and magmatic history. Global tomographic models show that elevated shear wavespeeds associated with the continental lithosphere extend to about ∼200 km depth beneath stable cratonic regions, and to much shallower depths beneath regions that have experienced deformation and magmatism (e.g. Romanowicz, 2009). In many locations, shear wave speed reductions across the base of the lithosphere (i.e. the lithosphere–asthenosphere boundary, henceforth LAB), occur over a sufficiently

narrow depth range to produce detectable conversions of shear-to-compressional (Sp) and compressional-to-shear (Ps) waves (e.g. Rychert et al., 2007; Li et al., 2007; Ford et al., 2010).

Ps and Sp conversions can be analyzed using the receiver-function method (for a recent summary, see Kind et al., 2012), to determine the depth to the seismically-defined LAB globally (e.g. Rychert and Shearer, 2009), as well as to estimate the velocity drop across it. While in tectonically and magmatically active regions, these depths and velocity drops tend to agree very well with the base of the lithosphere as determined from global seismic tomography, the depths are often incompatible with shear wave speed profiles beneath stable cratons and platforms (Lekić and Romanowicz, 2011). In these regions, the velocity gradients producing the strongest Ps and Sp conversions are typically associated with a mid-lithospheric discontinuity (henceforth, MLD),

whose physical cause and nature remains elusive (Fischer et al., 2010), but which may be related to a low-velocity zone within the lithosphere (e.g. Thybo and Perchuć, 1997; Lekic and Romanowicz, 2011) or a change in anisotropy (Yuan and Romanowicz, 2010).

Does this correspondence between thicker lithosphere and intra-lithospheric layering on one hand, and thinner lithosphere, deformation and magmatism on the other, persist down to the scale of physiographic units? The varied history of deformation and magmatism across the western United States makes it an ideal setting for studying this question. The compressional regime associated with, most recently, the Laramide orogeny during 75–35 Ma, was followed in the Neogene by extension and widespread magmatism (e.g. Bird, 1998; McQuarrie and Wernicke, 2005). This extension took on a wide mode in the Basin and Range, and narrower modes beneath the Rio Grande Rift to the east and the Salton Trough to the west (e.g. Buck, 1991). Yet, at the same time, the Colorado Plateau and the Wyoming craton underwent little internal deformation (e.g. Bird, 1979). Instead, the Colorado Plateau has uplifted by ∼2 km (Pederson et al., 2002), and been subjected to magmatic encroachment (Wenrich et al., 1995; Roy et al., 2009).

As the site of dense seismic station coverage provided by several temporary PASSCAL seismic experiments and the EarthScope Transportable Array, the western United States is also an ideal setting for seismic imaging of lithospheric structure variations on the scale of physiographic units. In this study, we employ Sp conversions to map variations in the depth to the seismic LAB and characterize the geographic distribution, strength, and depth-range of MLDs. The large quantity of available data makes possible the construction of common conversion-point stacks, which have previously been applied to image lithospheric thickness variations across the region (Levander and Miller, 2012) as well as focused lithospheric thinning beneath the Salton Trough (Lekic et al., 2011).

2. Data and method

We identify three-component seismic stations that operated in the study area with data available through the IRIS Data Management Center. These stations belong to 28 different permanent and temporary networks. Nevertheless, the vast majority of the usable records come from a handful of networks: the EarthScope USArray Transportable Array (TA) accounts for nearly 59% of the data, the United States National Seismic Network (US), Caltech Regional Seismic Network (CI), and the Rio Grande Seismic Transect (with extension, XM + XK) each contribute ∼8% of the data, the Intermountain West network 3.6%, and the Gobal Seismograph Network (GSN-IRIS/USGS: IU) and the Colorado BB-Array Lodore (XT) provide 2% each. In the Supplement, we discuss the relative contributions of the TA and other temporary networks in constraining variations in lithospheric structure across the region. For each station, we search the USGS NEIC global event catalog for events with Mw ⩾ 5.8, epicentral distances between 55° and 75°, and hypocenter depths <300 km. These selection parameters are chosen to minimize contamination of Sp receiver functions by interference with pPPP, pPPPP, sPPPP, SKS, and SKSp (Wilson et al., 2006), and to avoid effects of post-criticality of S waves at distances <55°. In total, our dataset includes 737 seismic stations contributing a total of 28,236 Sp receiver functions. The locations of the stations are denoted by triangles in Fig. 1, and they are colored according to the number of receiver functions obtained at the station. The waveforms are bandpass filtered between 0.03 and 0.25 Hz using a fourth order Butterworth filter, in which frequency range the S-to-P signal-to-noise ratio appears to be largest. We find that the use of a slightly smaller upper corner frequency (0.25 Hz) relative to that used by Abt et al. (2010) (0.50 Hz) yields somewhat cleaner images without adversely affecting accurate estimation of depths
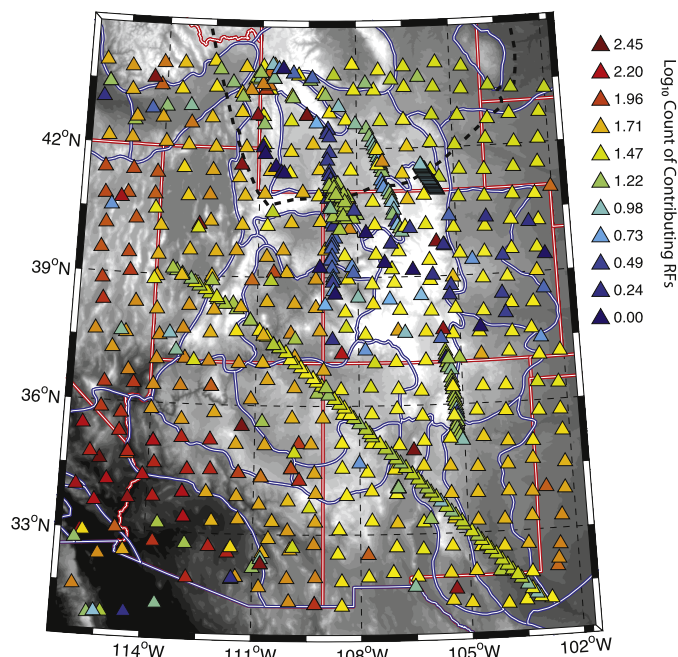

Fig. 1. Topographic map of study region showing the locations of stations used in the study (triangles), colored according to the base ten logarithm of the number of Sp receiver functions obtained at each station. Red lines are state boundaries, blue lines outline physiographic provinces of Fenneman and Johnson (1946), the dashed line traces the boundary of the Wyoming craton (Whitmeyer and Karlstrom, 2007). (For interpretation of the references to color in this figure legend, the reader is referred to the web version of this article.)

of lithospheric discontinuities. However, upper corners as small as 0.125 Hz often create interference between the Moho and shallow (<100 km) mantle phases (e.g. Hopper et al., submitted for publication).

Shear waves that traverse the outer core as compressional waves (SKS) and convert from shear to compressional waves in the mantle (SKS-to-P) are sometimes combined with Sp to map upper mantle discontinuities (e.g. Kind et al., 2012; Hansen et al., 2013). However, we found that including SKSp phases did not in general improve the clarity of phases observed in the common conversion point (CCP) stacks, and the results shown in this study are based on Sp phases alone.

In order to calculate Sp receiver functions, we use the semi-automatic data-processing technique developed by Abt et al. (2010) with two major improvements: (1) a new, array-based picking algorithm for the automatic identification of P and S arrivals necessary for accurate windowing of the parent and daughter waveforms prior to deconvolution; (2) implementation of deconvolution based on the extended time multi-taper correlation method. In the Supplement, we describe the array-picking algorithm, and compare its performance to the automatic algorithm of Abt et al. (2010), which has been broadly applied (e.g. Abt et al., 2010; Ford et al., 2010; Lekic et al., 2011). We demonstrate that the array-based picking algorithm more accurately identifies both P and S arrival times and is able to determine an arrival time for ∼30% more waveforms.

Once Sp receiver functions are obtained, they are combined into a 3D crust and mantle discontinuity model by common conversion point (CCP) stacking. First, receiver function amplitudes are migrated into a physical volume defined by depth, latitude and longitude (r, θ, ϕ), using 1D ray tracing along the backazimuth and ray parameter of the parent S phase and a velocity model for each station that is based on crustal V_p and V_p/V_s from the model of Lowry and Pérez-Gussinyé (2011, henceforth LPG) mantle V_s from the surface-wave and teleseismic body-wave travel-time model of
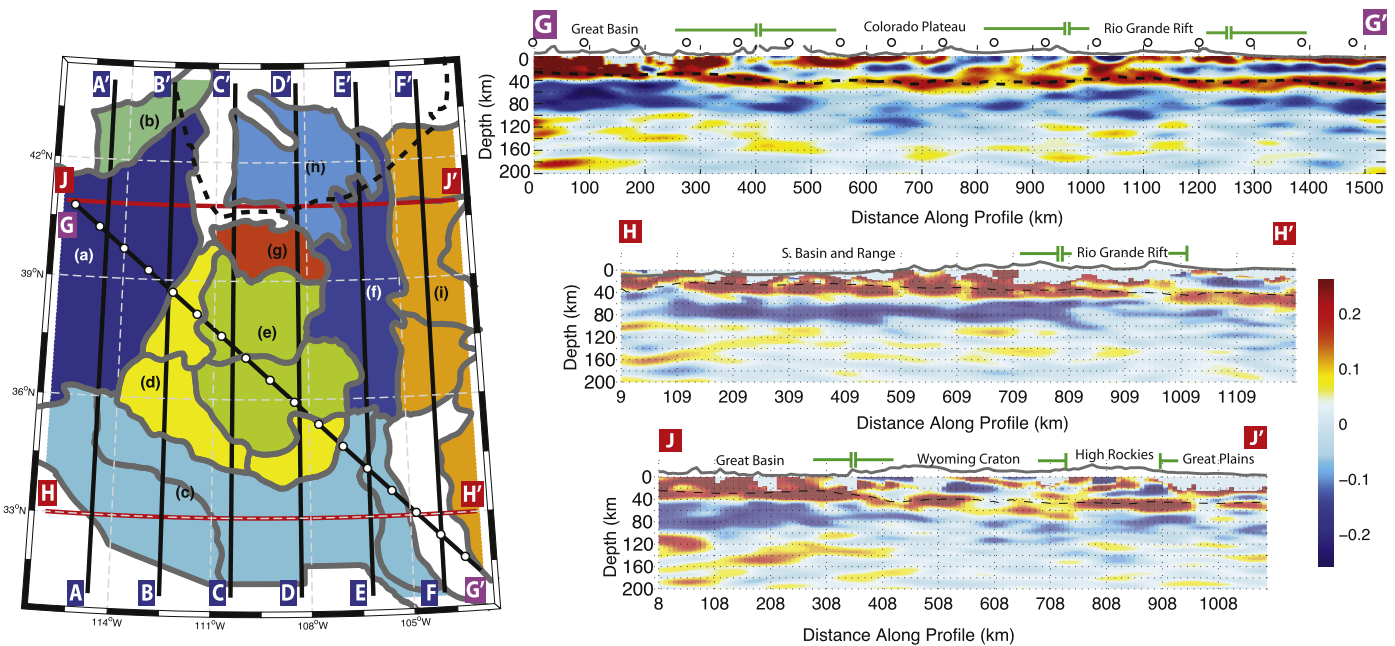
Fig. 2. (left) Map showing the surface traces of the vertical sections plotted in this figure and Fig. 3, as well as geographic extents of provinces used in Fig 4. (right) Vertical sections through Sp CCP stacks obtained using the new array-based picking algorithm presented in this paper (see Supplement). Warm (cool) colors indicate velocity increase (decrease) with depth and topography (black line) is exaggerated 10-fold. The dashed line traces the Moho from Lowry and Pérez-Gussinyé (2011). (For interpretation of the references to color in this figure legend, the reader is referred to the web version of this article.)

Obrebski et al. (2011), and mantle V_p from relative travel-times of teleseismic body waves model of Obrebski et al. (2010). The volume beneath the study region was discretized every 1 km in depth, and 0.1° in latitude and longitude. At each discrete location, the CCP stack was calculated by a weighted average of all receiver functions at that depth, where the weights are a function of the zero-offset Fresnel zone half-width for the depth of interest. In order to avoid poorly-constrained regions, we only calculate the weighted average when there are more than 35 receiver functions contributing to it. The definitions of weighting factors and stacking procedure are identical to that of Lekic et al. (2011).

3. Results

Vertical slices through the 3D crust and mantle discontinuity model are shown in Figs. 2 and 3. Warm (cool) colors correspond to areas where velocity increases (decreases) with depth sufficiently rapidly to produce an Sp conversion. In the Supplement, we compare the Sp CCP stacks obtained using the new array-based picking algorithm to those from the algorithm of Abt et al. (2010), and show that the array-based algorithm's increased accuracy results in more coherent images of lithospheric structure. By constructing CCP stacks using different subsets of data, we also show that Sp CCP stacks obtained using all available data and those obtained using data from only the Transportable Array (TA) yield similar constraints on lithospheric structure, indicating that the deployment and interstation spacing of the TA are sufficient for high quality imaging of the mantle lithosphere.

Fig. 3 shows that in nearly all locations, the largest-amplitude feature of the Sp CCP stacks, indicating a velocity increase with depth, corresponds to Mohorovičić discontinuity. Its depth is generally consistent with the depths inferred by Lowry and Pérez-Gussinyé (2011) using H-κ stacking of Ps receiver functions combined with gravity and surface heat-flow measurements. We stress that even though crustal thicknesses and V_p/V_s ratios from the LPG model are used to migrate to depth our Sp receiver functions, the agreement is meaningful because: (1) Sp receiver functions are constructed from different portions of the seismic waveforms;

(2) P waves converted from S waves traverse very different paths in the crust and upper mantle than S waves converted from P waves; (3) Sp conversions do not suffer from complications arising from arrivals that are multiply-reflected in shallow layers, such as the sediment or crust; (4) Sp receiver functions are dominated by longer period energy, with different lateral and depth sensitivities.

Beneath the strong positive Moho-related arrival in the CCP stacks, we observe a more distributed negative arrival that is associated with a negative velocity gradient (NVG) with depth. Forward modeling studies indicate that a velocity decrease of ∼5–10% over <30 km vertical distance is necessary to produce the Sp phases seen beneath much of the study area (e.g. Rychert et al., 2010; Fischer et al., 2010). The vertical sections in Figs. 2 and 3 show that both the depth and character of the NVG-related phase in the CCP stacks vary across the region of study. In particular, we observe:

- A prominent NVG at ∼70 km depth beneath the northern Great Basin (profile A, Fig. 3) and southern Basin and Range (profile H, Fig. 2), with hints of a rapid transition to depths of 40–50 km beneath the Salton Trough at the ends of the profiles;
- Gradual shallowing of the NVG going from the southern Basin and Range northward into the Great Basin (profile B, Fig. 3), consistent with the Sp results of Levander and Miller (2012);
- The NVG is weaker, deeper, and more distributed in depth beneath the central and northern Colorado Plateau, but is strong and shallow along its southern and western margins (profiles B–D, Fig. 3 and G, Fig. 2);
- The NVG is very weak and distributed to a depth of ∼150 km Wyoming craton (profiles C, D, E, Fig. 3 and J, Fig. 2);
- No obvious signs of localized lithospheric thinning beneath the northern segments of the Rio Grande Rift, where lithospheric thickness is similar to that beneath the Basin and Range (profile E, Fig. 3);
- The NVG is of intermediate strength and depth (80–90 km) beneath the High Rockies (profile E, Fig. 3);
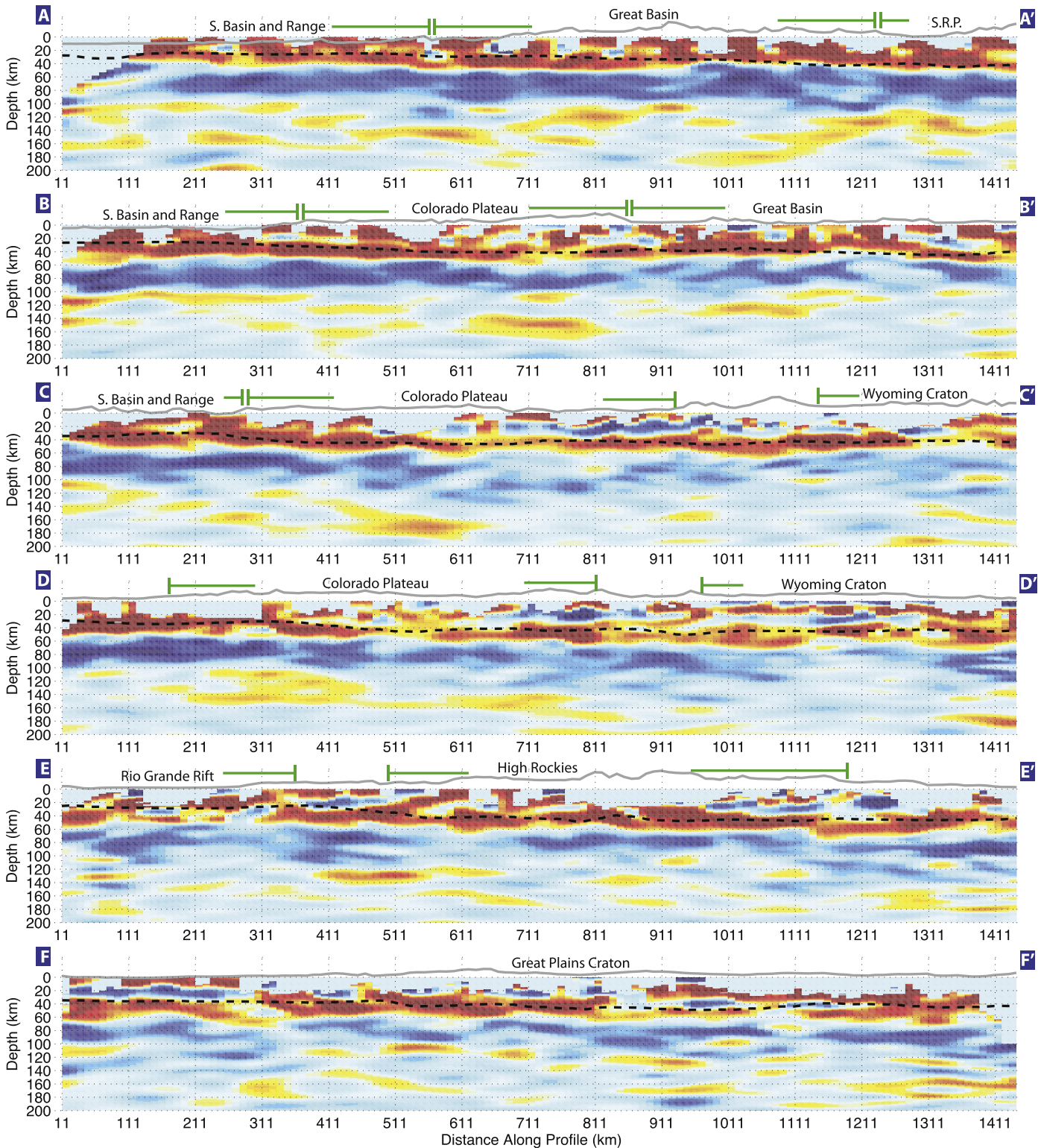
Fig. 3. Vertical sections through Sp CCP stacks, showing the variations in crustal and lithospheric thickness throughout the study region. Sections run south (left) to north (right) and move progressively eastward from top to bottom. Approximate surface extents of major physiographic provinces are denoted with green lines. Warm (cool) colors indicate velocity increase (decrease) with depth. For the surface trace of the sections, explanation of other markings, and the color scale, consult Fig. 2. (For interpretation of the references to color in this figure legend, the reader is referred to the web version of this article.)

- Significant NVG phases exist beneath the eastern margin of our study (the Great Plains craton), characterized by multiple NVGs distributed down to ~150 km depth (profile F, Fig. 3), although a single phase at 80–100 km depth is observed in certain areas.

The systematic differences in the character of NVG-related phases seen across different physiographic provinces are particularly apparent in Fig. 4, where we plot the average receiver functions for each of nine different regions, alongside absolute shear velocity profiles from two recent tomographic models (Obrebski
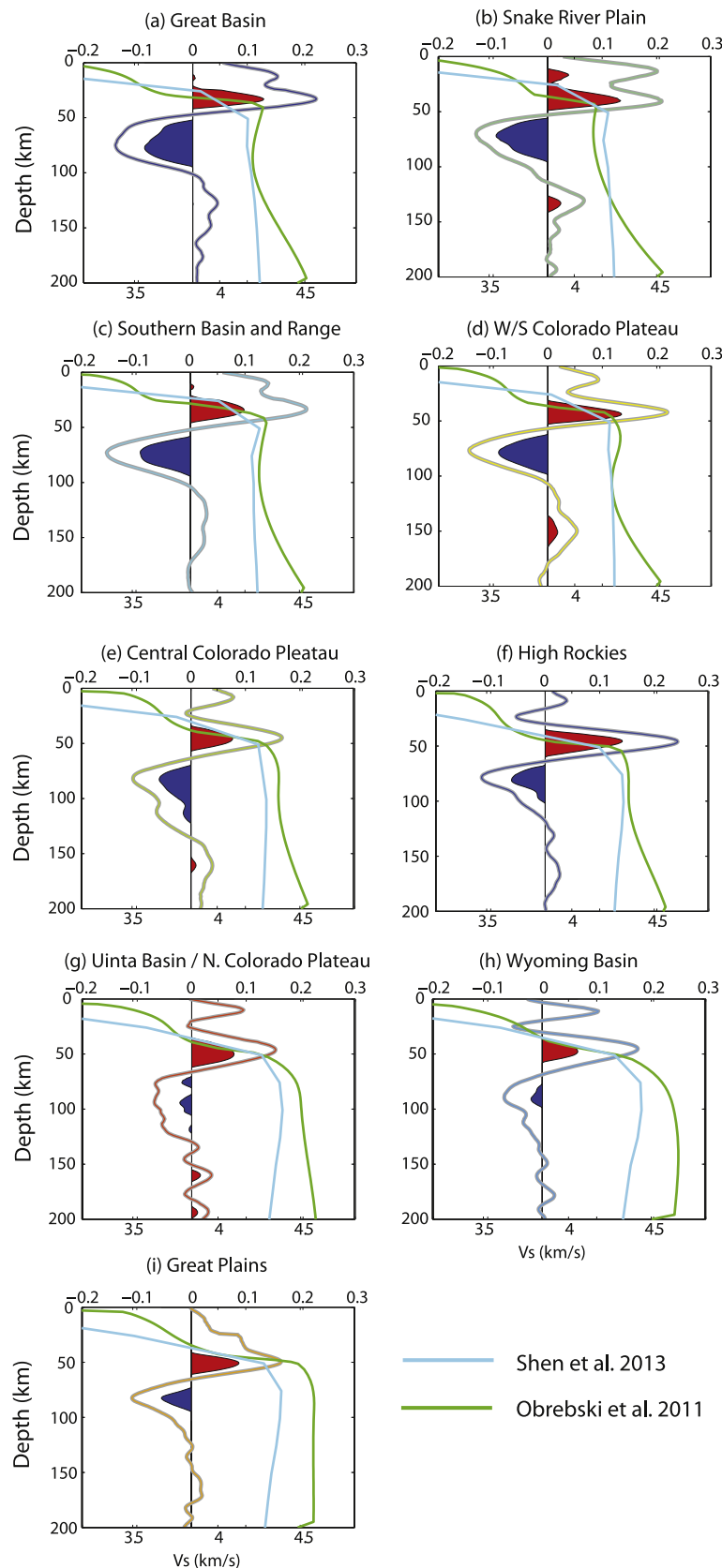
Fig. 4. Average Sp receiver functions for the main physiographic provinces (colored to match map of provinces in Fig. 2) plotted against the average absolute V_s profiles from two recent tomographic models of the western U.S. (Obrebski et al., 2011; Shen et al., 2013). Viewed in the context of absolute V_s profiles, the positive phase (red) in the Sp RFs can be associated with the Moho. The negative phase (blue) is less straightforward to interpret; beneath the Great Basin, Southern Basin and Range, the Snake River Plain, the High Rockies and the western and southern margins of the Colorado Plateau, is consistent with a seismically-defined lithosphere–asthenosphere boundary; beneath the Wyoming Basin (which corresponds to much of the Wyoming craton), the central and northern Colorado Plateau, and the Great Plains craton it likely represents mid-lithospheric discontinuity/ies. (For interpretation of the references to color in this figure legend, the reader is referred to the web version of this article.)
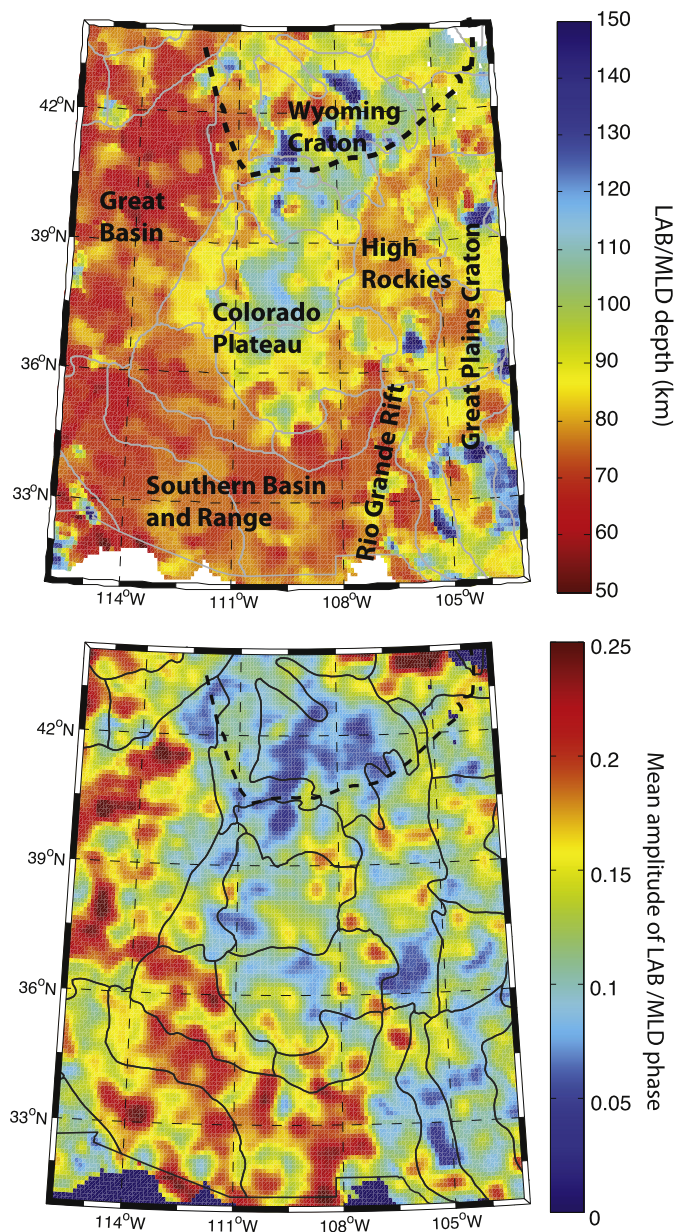
Fig. 5. (top) Map showing the depth of the negative velocity gradient phase, corresponding either to a seismically-defined lithosphere–asthenosphere boundary (LAB), or mid-lithospheric discontinuity (MLD). (bottom) Map of the amplitude of the Sp conversion produced across the MLD/LAB. Depths and amplitudes are automatically calculated from the Sp CCP stacks as the mean of the 20 most negative points in the 35–200 km depth range. Large amplitudes correspond to large velocity gradients across the LAB. Uncertainties associated with these maps are discussed in the Supplement.

et al., 2011; Shen et al., 2013). As with the CCP stacks, red indicates a velocity increase with depth (such as that across the Moho) and blue indicates a velocity decrease with depth (an NVG). However, we only color where the absolute amplitude of the receiver function is more than one standard deviation greater than zero; this way, two-thirds of intra-region variability in receiver functions is represented by the white area between the mean receiver function and the colored portion.

In Fig. 5, we plot the depth to and amplitude of the largest negative velocity gradients (NVG) from the Sp CCP stacks constructed using array-picked data. In order to avoid subjectivity in interpretating the CCP stacks, we use an automatic algorithm that defines the NVG amplitude as the mean amplitude and NVG depth as the

mean depth of the 20 most negative points in the 35–200 km depth range of the CCP profile beneath each point on the surface. When CCP values are unavailable on more than 10 km of the CCP profile or when no negative phase is observed, picks are not made. Fig. 5 shows that individual physiographic provinces can be identified with shallow (<75 km), intermediate-depth (80–90 km), or deep (>100 km) NVGs. Furthermore, provinces with greater LAB depths, which are primarily found within stable blocks such as the central Colorado Plateau, the Great Basin craton, and the Wyoming craton, tend to contain NVGs that are 2–3 times weaker than those beneath provinces with shallow LAB depths. In the Supplement, we describe a bootstrap analysis of the LAB depth and strength maps constructed using different random subsets of the complete dataset, and show that the differences in LAB depth and strength between individual physiographic provinces are robustly constrained.

4. Discussion

As the focus of this paper is variations in lithospheric thickness rather than crustal structure, we restrict our discussion of crustal features to a few brief points. Interestingly, we observe crustal thickening along the margins of the Wyoming craton (profile J, Fig. 2) that is not present in the LPG model. We interpret this as an indication of whole-crustal deformation that is localized at the margins of the thick and rigid lithosphere of the Wyoming craton, as previously reported by Levander and Miller (2012) and Hansen et al. (2013). We find that the Moho produces weak Sp conversions beneath parts of the Wyoming craton (profile J, Fig. 2), suggesting a reduced velocity contrast across the base of the crust, consistent with the results of Shen et al. (2013). We confirm that the Moho produces weak Sp conversions beneath central parts of the Colorado Plateau (profiles C and D, Fig. 3; Gilbert et al., 2007; Gilbert, 2012), and image complex lower-crustal arrivals (profile G, Fig. 2) previously noted by Levander et al. (2011) and Gilbert (2012), though discerning the likely Moho-related signals remains possible in our Sp CCP stacks. Beneath the Colorado Plateau, crustal thickness exceeds 40 km, with the Moho reaching depths of 50 km in places, in agreement with the previous Ps results (Lowry and Pérez-Gussinyé, 2011; Levander and Miller, 2012; Gilbert, 2012). Similar Moho depths are observed beneath the High Rockies, with a northward deepening of the Moho from ∼40 km to nearly 50 km (profile E, Fig. 3), consistent with previous Ps and Sp studies (Levander and Miller, 2012; Lowry and Pérez-Gussinyé, 2011); the northward deepening is particularly visible in the Ps results of Gilbert (2012). Because of their longer dominant periods, S-to-P conversions are unable to separate out signals arising from multiple, nearby, strong impedance contrasts. We see this beneath much of the Great Basin and the southern Basin and Range, where signal associated with the base of the crystalline basement interferes with that produced across the Moho, resulting in a merged positive phase in the CCP stacks that corresponds to neither the Moho nor the base of the crystalline basement.

The broad pattern of NVG depth variations obtained in this study (Fig. 5) agree with those from other recent Sp common conversion point investigations (Levander et al., 2011; Levander and Miller, 2012; Kumar et al., 2012; Hansen et al., 2013), but some features differ. Relatively shallow NVG depths beneath the Basin and Range and High Rockies and a deeper NVG beneath the central Colorado Plateau are common to Sp studies. However, while this study, Levander et al. (2011) and Kumar et al. (2012) all show the continuation of a relatively deep (100–120 km) NVG to the north of the Colorado Plateau (∼41°–42°N), this feature is not prominent in Levander and Miller (2012). Since this region tends to show multiple NVGs that are distributed in depth both in our (see

700–1100 km range of profile D, Fig. 3) and Levander and Miller (2012) Sp CCP stacks, discrepancies may result from picking different arrivals. NVG depths from Kumar et al. (2012) are smoother laterally than those in this study, and the depths they find in the Basin and Range are typically greater (ranging between 70 and 90 km). Hansen et al. (2013) image a NVG beneath the High Rockies at depths comparable to ours (∼80 km), but also report a deeper and weaker NVG at 150–170 km; we discuss this in more detail further in the subsection on the High Rockies.

4.1. Basin and Range, Great Basin, and the southern Rio Grande Rift

Shallow NVGs are observed beneath the southern Basin and Range, the Great Basin, and the southern portion of the Rio Grande Rift. The negative velocity gradients implied by these phases fall within the transition from higher velocity lithospheric lid to asthenospheric low velocity zone in the shear velocity models from combined surface and body wave tomography of Obrebski et al. (2011) (Fig. 4) and are thus interpretable as the seismically-defined LAB. The amplitudes of these phases are larger than elsewhere in our study region, indicating larger LAB velocity gradients, similar in magnitude to the ∼8% drop in V_s inferred from Sp RFs beneath Southern California by Lekic et al. (2011); the V_s drop would have to be larger by about 50% if it were to be distributed across 20 km in depth (see Fig. 4 of Rychert et al., 2010, for more detail). The large LAB velocity gradients suggested by large-amplitude phases in our CCP stacks, coupled with low asthenospheric shear velocities (e.g. Schmandt and Humphreys, 2010; Obrebski et al., 2011; Rau and Forsyth, 2011; Gao et al., 2004), are consistent with the presence of partial melt in the asthenosphere.

Given the substantial extension and magmatic activity that the Basin and Range and southern Rio Grande Rift experienced since the Miocene (e.g. Chapin and Cather, 1994; McQuarrie and Wernicke, 2005), their shallow LAB is consistent with lithospheric thinning due to stretching and magmatic erosion. We find that average lithospheric thickness beneath the Northern Basin and Range is ∼10 km less than the 70 km average thickness detected beneath the Southern Basin and Range; this is consistent with the elevation and Bouger gravity anomaly differences between the two provinces (e.g. Parsons et al., 1994). Lithospheric thicknesses beneath the southern Rio Grande Rift are similar to those found beneath the southern Basin and Range, consistent with distributed extension, but markedly different from the highly localized lithospheric thinning reported beneath the Salton Trough and Inner Continental Borderland (Lekic et al., 2011). The lack of laterally abrupt lithospheric thinning beneath the Rio Grande Rift agrees with both the distributed crustal deformation inferred from Ps receiver function images of the Moho (Wilson et al., 2005), and the diffuse nature of geodetically-measured present-day extension across the region (Berglund et al., 2012). In the southern Rio Grande Rift, where ∼50% extension has occurred (Chapin and Cather, 1994) some xenoliths from depths of ∼45 km have compositions indicative of depleted Proterozoic mantle while others suggest the presence of young, convecting asthenospheric mantle, implying that a portion of the original mantle lithosphere has been removed (Byerly and Lassiter, 2012). Indeed, below this area (∼850 km on profile H, Fig. 2), the LAB-related NVG is locally disrupted and low amplitude, a result that is consistent with lithospheric removal to depths just below the Moho.

4.2. Colorado Plateau, Wyoming Craton, and the Great Plains Craton

Beneath the central and northern Colorado Plateau, Wyoming craton, and the Great Plains craton along the eastern margin of our study region, regional body- and surface-wave tomography (e.g. Obrebski et al., 2011; Liu et al., 2011; Yuan et al., 2011; Bailey et al., 2012) suggests that relatively fast velocities extend to depths greater than most of the NVG phase(s) (see Fig. 4). Therefore, in these regions we interpret most of the NVGs seen in our CCP stacks to be mid-lithospheric discontinuities, similar to those observed using Ps and Sp receiver functions beneath other stable continental regions (e.g. Rychert and Shearer, 2009; Abt et al., 2010; Ford et al., 2010). However, in some cases an NVG lies at a depth great enough to be consistent with the seismically-defined LAB, similar to the conclusions of Hansen et al. (2013) for the Great Plains. The NVGs beneath the central/north Colorado Plateau, Wyoming craton, and Great Plains are typically weaker than the NVGs in the Basin and Range and southern Rio Grande Rift, and NVGs at multiple depths are often observed, although examples of single mid-lithospheric NVGs also occur. While the complexity of mid-lithospheric NVG-related phases makes direct inference of velocity drops difficult, the fact that average amplitudes of NVG phases are a factor of 2–3 weaker than those we detect beneath actively extending regions implies a ∼3% V_s drop across a given mid-lithospheric discontinuity. Alternatively, velocity drops beneath the central/north Colorado Plateau, Wyoming craton, and Great Plains could be distributed over larger depth ranges than beneath neighboring extended lithosphere.

The lithosphere of the Colorado Plateau is thickest near its center and in its north (Uinta Basin), where NVGs interpretable as the LAB are observed in the 110–130 km range (see Fig. 4). This depth for the LAB is comparable to the depth extent of cool, depleted lithosphere inferred from xenoliths sampling the central Colorado Plateau (Riter and Smith, 1996; Lee et al., 2001) that were erupted toward the end of the ignimbrite flare-up, thought to be associated with the removal of the Farallon slab. Furthermore, it is broadly consistent with the Sp images of both Levander and Miller (2012) and Kumar et al. (2012) and the joint receiver function and surface-wave inversions of Bailey et al. (2012). The depth of the NVG shallows beneath the western, southern, and southeastern regions of the Colorado Plateau (Fig. 3, profiles B, C and D, and Fig. 5). The shallow (70–80 km) NVGs observed beneath the entire south/southwestern portion of the Plateau is in agreement both with melt equilibration pressures of ∼100 km from the southwestern Plateau (Lee et al., 2009), and with recent isotopic analysis that attributes recent volcanism to decompression melting to depths of <75 km (Reid et al., 2012).

The fact that NVG depths beneath the western, southern, and southeastern margins of the Colorado Plateau are indistinguishable from those in the nearby Basin and Range could be interpreted to suggest that these regions have experienced substantial lithospheric thinning. However, while the margins of the Colorado Plateau have experienced minor deformation (e.g. Kreemer et al., 2010; Berglund et al., 2012), this tectonic block has been largely undeformed throughout the first compressional and then extensional deformational history of the broader western U.S. (e.g. Bird, 1979). Therefore, the thinner lithosphere at the margins of the Plateau is more consistent with thermal and magmatic erosion of the lithosphere during the Cenozoic (Roy et al., 2009; Crow et al., 2011), rather than mechanical stretching. While we do not see a clear expression in the Sp CCP images of proposed ongoing lithospheric downwelling beneath the Colorado Plateau (Levander et al., 2011), our images cannot by themselves rule out such a possibility. Interestingly, the thinning of the southeastern portion of the Colorado Plateau lithosphere matches the spatial extent of the density deficit determined from joint modeling of gravity and topography data (Roy et al., 2005).

4.3. High Rockies

Intermediate depth (80–90 km) NVGs are observed beneath the High Rockies. Should this NVG phase be interpreted as the

seismically-defined LAB, or an especially coherent and high-amplitude MLD? To answer this question, we compare the velocity structure beneath the High Rockies to that of surrounding regions. Without exception, high resolution tomographic studies find that at mantle lithospheric depths (50–150 km) both V_s (e.g. Schmandt and Humphreys, 2010; Liu et al., 2011; Obrebski et al., 2011; Hansen et al., 2013; Shen et al., 2013) and V_p (e.g. Schmandt and Humphreys, 2010; Burdick et al., 2010) are slower beneath the High Rockies than beneath the central Colorado Plateau, the Wyoming craton, or the Great Plains craton; indeed, the V_s and V_p anomaly beneath the southern High Rockies is similar to that observed beneath the margins of the Colorado Plateau, where the NVG can be unambiguously associated with the seismically-defined LAB. Furthermore, Pn phases, which are sensitive to mantle velocities directly beneath the Moho, Buehler and Shearer (2012) find that the shallow mantle lithosphere beneath the High Rockies is significantly slower than the lithospheres of the central Colorado Plateau, Wyoming craton, and Great Plains craton, and is comparable to the shallow mantle found beneath the northern Rio Grande Rift. Based on these independent lines of evidence, we interpret the NVG phase beneath the High Rockies as the seismically-defined LAB. This interpretation is also consistent with reduced elastic thickness inferred from correlation of gravity and topography data and very high surface heatflow (Blackwell and Richards, 2004; Reiter, 2008).

Other converted phase studies of the region have inferred intermediate thickness (80–100 km) lithosphere beneath the High Rockies (Liu et al., 2011; Levander and Miller, 2012; Kumar et al., 2012; Bailey et al., 2012). An exception is the work of Hansen et al. (2013), who detect a large negative Sp phase at depths of 70–100, but interpret a second, weaker negative Sp phase at 150–170 km as the LAB. It is important to note that our interpretation of the clear NVG at ∼80–90 km depth as the seismically-defined LAB, implies only that it is the top of a relatively low velocity layer consisting of weak mantle material; the origin of this material cannot be determined from seismology alone. In this region, the weak sub-LAB material could either be original continental lithosphere that has now been altered, or modern, convecting asthenosphere. In either case, the absence of significant extension in the High Rockies (Chapin and Cather, 1994) again implies that magmatic and thermal erosion, as opposed to mechanical extension, must have played a key role in attaining the relatively shallow lithospheric thickness. Interestingly, the NVG appears to be absent beneath the southernmost Rockies (500–700 km on profile E of Fig. 3) where some tomography models (Li et al., 2005; Obrebski et al., 2011; Shen et al., 2013) found anomalously low shear wave speeds in the 60–100 km depth range. The zone of missing NVG is approximately spatially correlated with the intersection between the Rockies and the Jemez Lineament, a band of mid-Miocene to recent magmatism, and may also relate to the overlap between the southern Rockies and the northern end of the Rio Grande Rift.

5. Conclusions

The varied deformation history of the Western United States provides an ideal setting in which to study the relationship between lithospheric structure and deformation. In order to take full advantage of deployments of dense seismic arrays in the region, we develop, validate, and apply a new array-based picking algorithm to generate over 28,000 Sp receiver functions. When mapped into the three-dimensional volume beneath the region via common conversion point (CCP) stacking, the Sp receiver functions yield an image of velocity interfaces associated with the lithosphere–asthenosphere boundary (LAB) as well as mid-lithospheric discontinuities (MLDs).

We show that the more reliable S arrival picks obtained with the array-based picker result in more coherent CCP stacks. By comparing Sp CCP stacks obtained using all available data with those obtained using data from the Transportable Array (TA) alone, we demonstrate that the length of deployment, noise levels, and inter-station spacing is sufficient to yield clear and interpretable images of lithospheric structure.

We find that the Western United States is characterized by a wide range of lithospheric structures, with differences in lithospheric thickness and the strength of the seismic expression of the lithosphere–asthenosphere boundary persisting down to the scale of single physiographic units. The main conclusions are schematically shown in the graphical abstract:

- Beneath areas that have undergone substantial extension in the Neogene—including the eastern Great Basin, the southern Basin and Range, and the southern Rio Grande Rift—we detect strong Sp conversions across a relatively shallow (60–80 km) seismically-defined LAB.
- We detect Sp conversions across a discontinuity at depths of 80–90 km beneath the High Rockies, which we interpret as the seismically-defined LAB.
- Beneath areas that have remained relatively undeformed—including the Wyoming craton and the Great Plains craton—we detect Sp conversions in the 90–140 km depth range that are substantially weaker and more distributed in depth than those beneath less stable regions.
- Beneath the Colorado Plateau, Sp CCP stacks show that lithospheric thinning has accompanied magmatic encroachment, so that the lithosphere beneath the margins of the Plateau produces Sp conversions indistinguishable from those beneath surrounding extensional provinces. The central and northern portions of the Plateau, on the other hand, produce weak Sp conversions in the 90–140 km depth range.

The clear association between lithospheric thickness, magmatic encroachment, and deformation history provides a self-consistent framework to explain the observed variations in Sp phase depths and character; therefore, we do not find it necessary to invoke the fragmentation and preferential preservation of the Farallon slab beneath the Colorado Plateau, the Wyoming craton and the Great Plains craton, as has previously been suggested (Kumar et al., 2012).

The observed variations in lithospheric structure across structural blocks with different magmatic and deformational histories imply that:

1. Both mechanical thinning and magmatic and thermal erosion have likely contributed to the thin lithosphere observed in the Basin and Range and southern Rio Grande Rift.
2. At the margins of the Colorado Plateau and beneath the High Rockies, where extension has been relatively minor, strong and shallow seismic LABs indicate magmatic alteration of the lithosphere.
3. Mid-lithospheric discontinuities seen in comparatively thick, stable lithosphere produce weaker Sp conversions and are often more distributed in depth than seismically-observed LABs in regions of thin lithosphere.
4. Mid-lithospheric discontinuities and weak, deep phases consistent with a seismic LAB are sometimes observed together.

Appendix A. Supplementary material

Supplementary material related to this article can be found online at http://dx.doi.org/10.1016/j.epsl.2013.11.026.

References

Abt, D., Fischer, K., French, S., Ford, H., Yuan, H., Romanowicz, B., 2010. North American lithospheric discontinuity structure imaged by Ps and Sp receiver functions. J. Geophys. Res. 115 (B09301). http://dx.doi.org/10.1029/2009JB006914.

Bailey, I.W., Miller, M.S., Liu, K., Levander, A., 2012. V_s and density structure beneath the Colorado Plateau constrained by gravity anomalies and joint inversions of receiver function and phase velocity data. J. Geophys. Res. 117, B02313. http://dx.doi.org/10.1029/2011JB008522.

Berglund, H., Sheehan, A., Murray, M., Roy, M., Lowry, A., Nerem, R., Blume, F., 2012. Distributed deformation across the Rio Grande Rift, Great Plains, and Colorado Plateau. Geology 40 (1), 23–26.

Bird, P., 1979. Continental delimitation and the Colorado Plateau. J. Geophys. Res. 84 (B13), 7561–7571.

Bird, P., 1998. Kinematic history of the Laramide orogeny in latitudes 35°–49°N, western United States. Tectonics 17 (5), 780–801.

Blackwell, D., Richards, M., 2004. Geothermal map of North America. Am. Assoc. Petroleum Geologist (AAPG). Product code 423, scale 1:6,500,000.

Buck, W.R., 1991. Modes of continental lithospheric extension. J. Geophys. Res. 96 (B12), 20,161–20,178.

Buehler, J., Shearer, P., 2012. Localized imaging of the uppermost mantle with USArray Pn data. J. Geophys. Res. 117 (B9). http://dx.doi.org/10.1029/2012JB009.

Burdick, S., van der Hilst, R.D., Vernon, F.L., Martynov, V., Cox, T., Eakins, J., Karasu, G.H., Tylell, J., Astiz, L., Pavlis, G.L., 2010. Model update January 2010: Upper mantle heterogeneity beneath North America from traveltime tomography with global and USArray transportable array data. Seismol. Res. Lett. 81 (5), 689–693.

Byerly, B.L., Lassiter, J.C., 2012. Evidence from mantle xenoliths for lithosphere removal beneath the central Rio Grande Rift. Earth Planet. Sci. Lett. 355, 82–93.

Chapin, C.E., Cather, S.M., 1994. Tectonic setting of the axial basins of the northern and central Rio Grande Rift. Spec. Pap., Geol. Soc. Am. 291, 5–26.

Crow, R., Karlstrom, K., Asmerom, Y., Schmandt, B., Polyak, V., DuFrane, S.A., 2011. Shrinking of the Colorado Plateau via lithospheric mantle erosion: Evidence from Nd and Sr isotopes and geochronology of Neogene basalts. Geology 39 (1), 27–30.

Fenneman, N., Johnson, D., 1946. Physical divisions of the United States: US Geological Survey map prepared in cooperation with the physiographic commission. US Geological Survey. Scale 1:7,000,000.

Fischer, K., Ford, H., Abt, D., Rychert, C., 2010. The lithosphere–asthenosphere boundary. Annu. Rev. Earth Planet. Sci. 38, 551–575.

Ford, H., Fischer, K., Abt, D., Rychert, C., Elkins-Tanton, L., 2010. The lithosphere–asthenosphere boundary and cratonic lithospheric layering beneath Australia from Sp wave imaging. Earth Planet. Sci. Lett. 300 (3), 299–310.

Gao, W., Grand, S.P., Baldridge, W.S., Wilson, D., West, M., Ni, J.F., Aster, R., 2004. Upper mantle convection beneath the central Rio Grande Rift imaged by P and S wave tomography. J. Geophys. Res. 109, B03305. http://dx.doi.org/10.1029/2003JB002743.

Gilbert, H., 2012. Crustal structure and signatures of recent tectonism as influenced by ancient terranes in the western United States. Geosphere 8 (1), 141–157.

Gilbert, H., Velasco, A., Zandt, G., 2007. Preservation of Proterozoic terrane boundaries within the Colorado Plateau and implications for its tectonic evolution. Earth Planet. Sci. Lett. 258 (1), 237–248.

Hansen, S., Dueker, K., Stachnik, J., Aster, R., Karlstrom, K., 2013. A rootless rockies—Support and lithospheric structure of the Colorado Rocky Mountains inferred from CREST and TA seismic data. Geochem. Geophys. Geosyst. 14 (8), 2670–2695. http://dx.doi.org/10.1002/ggge.20143.

Hopper, E., Ford, H.A., Fischer, K.M., Lekic, V., Fouch, M.J., submitted for publication. The lithosphere–asthenosphere boundary and the tectonic and magmatic history of the northwestern United States. Earth Planet. Sci. Lett.

Kind, R., Yuan, X., Kumar, P., 2012. Seismic receiver functions and the lithosphere–asthenosphere boundary. Tectonophysics 536–537, 25–43.

Kreemer, C., Blewitt, G., Bennett, R.A., 2010. Present-day motion and deformation of the Colorado Plateau. Geophys. Res. Lett. 37 (L10311). http://dx.doi.org/10.1029/2010GL043374.

Kumar, P., Yuan, X., Kind, R., Mechie, J., 2012. The lithosphere–asthenosphere boundary observed with USArray receiver functions. Solid Earth 3, 149–159.

Lee, C.-T., Yin, Q., Rudnick, R.L., Jacobsen, S.B., 2001. Preservation of ancient and fertile lithospheric mantle beneath the southwestern United States. Nature 411 (6833), 69–73.

Lee, C.-T.A., Luffi, P., Plank, T., Dalton, H., Leeman, W.P., 2009. Constraints on the depths and temperatures of basaltic magma generation on earth and other terrestrial planets using new thermobarometers for mafic magmas. Earth Planet. Sci. Lett. 279 (1), 20–33.

Lekic, V., Romanowicz, B., 2011. Tectonic regionalization without a priori information: A cluster analysis of upper mantle tomography. Earth Planet. Sci. Lett. 308 (1), 151–160.

Lekic, V., French, S., Fischer, K., 2011. Lithospheric thinning beneath rifted regions of southern California. Science 334 (6057), 783–787.

Levander, A., Miller, M., 2012. Evolutionary aspects of lithosphere discontinuity structure in the western US. Geochem. Geophys. Geosyst. 13 (7), Q0AK07. http://dx.doi.org/10.1029/2012GC004056.

Levander, A., Schmandt, B., Miller, M., Liu, K., Karlstrom, K., Crow, R., Lee, C., Humphreys, E., 2011. Continuing Colorado Plateau uplift by delamination-style convective lithospheric downwelling. Nature 472 (7344), 461–465.

Li, A., Forsyth, D., Fischer, K., 2005. Rayleigh wave constraints on shear-wave structure and azimuthal anisotropy beneath the Colorado Rocky Mountains. Geophys. Monogr. 154, 385–401.

Li, X., Yuan, X., Kind, R., 2007. The lithosphere–asthenosphere boundary beneath the western United States. Geophys. J. Int. 170 (2), 700–710.

Liu, K., Levander, A., Niu, F., Miller, M.S., 2011. Imaging crustal and upper mantle structure beneath the Colorado Plateau using finite frequency Rayleigh wave tomography. Geochem. Geophys. Geosyst. 12 (7). http://dx.doi.org/10.1029/2011GC003611.

Lowry, A., Pérez-Gussinyé, M., 2011. The role of crustal quartz in controlling Cordilleran deformation. Nature 471 (7338), 353–357.

McQuarrie, N., Wernicke, B., 2005. An animated tectonic reconstruction of southwestern North America since 36 Ma. Geosphere 1 (3), 147–172.

Obrebski, M., Allen, R., Xue, M., Hung, S., 2010. Slab-plume interaction beneath the Pacific northwest. Geophys. Res. Lett. 37, L14305. http://dx.doi.org/10.1029/2010GL043489.

Obrebski, M., Allen, R., Pollitz, F., Hung, S., 2011. Lithosphere–asthenosphere interaction beneath the western United States from the joint inversion of body-wave traveltimes and surface-wave phase velocities. Geophys. J. Int. 185 (2), 1003–1021.

Parsons, T., Thompson, G.A., Sleep, N.H., 1994. Mantle plume influence on the Neogene uplift and extension of the US western Cordillera?. Geology 22 (1), 83–86.

Pederson, J.L., Mackley, R.D., Eddleman, J.L., 2002. Colorado Plateau uplift and erosion evaluated using GIS. GSA Today 12 (8), 4–10.

Rau, C.J., Forsyth, D.W., 2011. Melt in the mantle beneath the amagmatic zone southern Nevada. Geology 39 (10), 975–978.

Reid, M.R., Bouchet, R.A., Blichert-Toft, J., Levander, A., Liu, K., Miller, M.S., Ramos, F.C., 2012. Melting under the Colorado Plateau, USA. Geology 40 (5), 387–390.

Reiter, M., 2008. Geothermal anomalies in the crust and upper mantle along southern Rocky Mountain transitions. Geol. Soc. Am. Bull. 120 (3–4), 431–441.

Riter, J., Smith, D., 1996. Xenolith constraints on the thermal history of the mantle below the Colorado Plateau. Geology 24 (3), 267–270.

Romanowicz, B., 2009. The thickness of tectonic plates. Science 324 (5926), 474–476.

Roy, M., MacCarthy, J., Selverstone, J., 2005. Upper mantle structure beneath the eastern Colorado Plateau and Rio Grande Rift revealed by Bouguer gravity, seismic velocities, and xenolith data. Geochem. Geophys. Geosyst. 6, Q10007. http://dx.doi.org/10.1029/2005GC001008.

Roy, M., Jordan, T., Pederson, J., 2009. Colorado Plateau magmatism and uplift by warming of heterogeneous lithosphere. Nature 459 (7249), 978–982.

Rychert, C., Shearer, P., 2009. A global view of the lithosphere–asthenosphere boundary. Science 324 (5926), 495–498.

Rychert, C., Rondenay, S., Fischer, K., 2007. P-to-S and S-to-P imaging of a sharp lithosphere–asthenosphere boundary beneath eastern North America. J. Geophys. Res. 112, B08314. http://dx.doi.org/10.1029/2006JB004619.

Rychert, C.A., Shearer, P.M., Fischer, K.M., 2010. Scattered wave imaging of the lithosphere–asthenosphere boundary. Lithos 120 (1), 173–185.

Schmandt, B., Humphreys, E., 2010. Complex subduction and small-scale convection revealed by body-wave tomography of the western United States upper mantle. Earth Planet. Sci. Lett. 297 (3), 435–445.

Shen, W., Ritzwoller, M., Schulte-Pelkum, V., 2013. A 3-d model of the crust and uppermost mantle beneath the central and western US by joint inversion of receiver functions and surface wave dispersion. J. Geophys. Res. 118, 262–276. http://dx.doi.org/10.1029/2012JB009602.

Thybo, H., Perchuć, E., 1997. The seismic 8° discontinuity and partial melting in continental mantle. Science 275 (5306), 1626–1629.

Wenrich, K.J., Billingsley, G.H., Blackerby, B.A., 1995. Spatial migration and compositional changes of Miocene-quaternary magmatism in the western Grand Canyon. J. Geophys. Res. 100 (B7), 10,417–10,440.

Whitmeyer, S.J., Karlstrom, K.E., 2007. Tectonic model for the Proterozoic growth of North America. Geosphere 3 (4), 220–259.

Wilson, D., Aster, R., West, M., Ni, J., Grand, S., Gao, W., Baldridge, W., Semken, S., Patel, P., 2005. Lithospheric structure of the Rio Grande Rift. Nature 433 (7028), 851–855.

Wilson, D., Angus, D., Ni, J., Grand, S., 2006. Constraints on the interpretation of S-to-P receiver functions. Geophys. J. Int. 165 (3), 969–980.

Yuan, H., Romanowicz, B., 2010. Lithospheric layering in the North American Craton. Nature 466, 1063–1068.

Yuan, H., Romanowicz, B., Fischer, K.M., Abt, D., 2011. 3-D shear wave radially and azimuthally anisotropic velocity model of the North American upper mantle. Geophys. J. Int. 184 (3), 1237–1260.